



**HAL**  
open science

# Effect of notch root radius on the creep failure mechanisms on polyamide 6 : application of fracture mechanics approaches

Lucien Laiarinandrasana, Cédric Regrain

► **To cite this version:**

Lucien Laiarinandrasana, Cédric Regrain. Effect of notch root radius on the creep failure mechanisms on polyamide 6 : application of fracture mechanics approaches. Fracture of materials and structures from micro to macro scale - ECF 18, Aug 2010, Dresden, Germany. 8 p. hal-00541275

**HAL Id: hal-00541275**

**<https://minesparis-psl.hal.science/hal-00541275>**

Submitted on 5 Jun 2013

**HAL** is a multi-disciplinary open access archive for the deposit and dissemination of scientific research documents, whether they are published or not. The documents may come from teaching and research institutions in France or abroad, or from public or private research centers.

L'archive ouverte pluridisciplinaire **HAL**, est destinée au dépôt et à la diffusion de documents scientifiques de niveau recherche, publiés ou non, émanant des établissements d'enseignement et de recherche français ou étrangers, des laboratoires publics ou privés.

# **EFFECT OF NOTCH ROOT RADIUS ON THE CREEP FAILURE MECHANISMS ON PALLYAMIDE 6: APPLICATION OF FRACTURE MECHANICS APPROACHES**

L. Laiarinandrasana, C. Regrain

MINES ParisTech, MAT-Centre des Matériaux, UMR CNRS 7633, B.P. 87  
91003 Evry Cedex, France

## **ABSTRACT**

The polyamide 6 (PA6) under study exhibits non-linear time dependent (viscoplastic) deformation when submitted to steady load (creep) at room temperature. An experimental database consisting of creep tests performed on notched round bars with various notch root radii was built. Failure mechanisms of the PA6 material were investigated thanks to comprehensive microscopic examinations of deformed and broken specimens. Global approach of fracture mechanics for creeping solids was applied and showed its limits. Alternatively, the local approach of fracture mechanics was attempted, with the help of finite element analysis. It was shown that this approach could successfully capture main features of creep damage mechanisms of the PA6 material, which lead to complete failure.

## **KEYWORDS**

Polyamide 6, Creep fracture, Fracture mechanics, Finite Element, Local approach, Damage mechanics, Void growth, Cavitation, Polymer mechanics

## **INTRODUCTION**

Polyamide 6 (PA6) is a semi-crystalline polymer utilised in many structural components. At room temperature, PA6 exhibits non-linear time dependent (viscoplastic) deformation. The engineering component made of the PA6 under study is submitted to steady load (creep). Thus, the motivation of this work is to investigate failure mechanisms of the PA6 material under creep loading, as well as to propose models accounting for such mechanisms.

To this end, an experimental database consisting of creep tests carried out on notched round bars with various notch root radii was constituted. The stress triaxiality ratio parameter is introduced to specify the stress state in the cross-section of the specimens, according to the notch root radius. Notch opening displacement vs. time was recorded for each creep test. A video camera was installed in order to monitor the shape of the notch during the test. Microscopic examinations of fracture surfaces were carried out to investigate deformation and damage mechanisms.

The global approach of fracture mechanics for creeping solids was applied for experimental data on assumed (sharp) cracked round bars. A master curve can be determined using this approach but it cannot account for failure mechanisms. The local approach of fracture mechanics was then attempted, with the help of finite element modelling. The simulation of creep tests on two specific notched specimens could successfully predict the location of the maximum damage, within the cross section.

## **MATERIAL, SPECIMEN AND TESTING**

The PA6 material of interest was provided by Angst & Pfister as 610mmx1230mm flow moulded plates with 10mm in thickness [1]. The main physical-chemical properties of this PA6 material are as follows: the glass transition temperature  $T_g = 53^\circ\text{C}$ , the melting point  $T_F = 219^\circ\text{C}$  and crystallinity index  $z = 43\%$  were obtained with the help of Modulated Differential Scanning Calorimeter (MDSC). The Young's modulus at room temperature  $E = 2850\text{MPa}$  was estimated with the initial slope of the stress-strain curve.

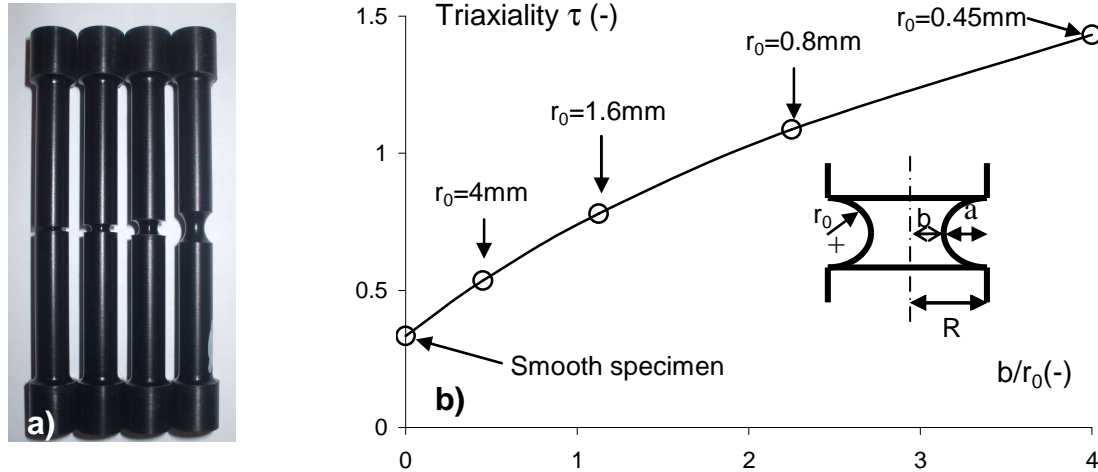


Figure 1: Specimens and specific parameters

Specimens consisted of notched round bars (figure 1a) with machined notch root radii  $r_0$ : 0.45mm, 0.8 mm, 1.6mm and 4mm [2]. According to the value of  $r_0$ , the specimens will be noted as  $NTr_0$  for “Notched Tensile  $r_0$ ”. All notched round bars have the same minimal section radius with  $b = 1.8\text{mm}$  and the same nominal radius  $R = 3.6\text{mm}$  (Figure 1b). Reducing  $r_0$  results in increasing the stress triaxiality ratio  $\tau$  defined as follows [3]:

$$\tau = \frac{1}{3} + \ln\left(1 + \frac{b}{2r_0}\right) \quad (1)$$

Equation 1 is the expression of the maximum stress triaxiality ratio located in the centre of the specimen. This parameter, which also represents the mean stress, will be extensively used in the paper. Its value for classical uniaxial tensile specimen is 0.33 as it can be seen in figure 2b.

Creep tests with various applied loads were performed on these specimens in order to study the effects of stress triaxiality on damage and failure of the PA6 at room temperature. The creep notch opening displacement as well as the load were recorded with respect to time. Since the study focuses on creep regime, the loading stage is subtracted in all experimental data. Furthermore, a video camera was installed for several tests in order to examine any specific events occurring during the creep test. These events allowed further analyses of the deformation and damage mechanisms.

## EXPERIMENTAL RESULTS

### Time to failure versus stress triaxiality ratio

Figure 2 displays the time to failure ( $T_f$ ) against the stress triaxiality  $\tau$  for each specimen, parameterized by the applied net stress. Only tests at 70MPa and 74MPa were represented

for the sake of clarity in figure 2, the trends being the same for other applied loads. The notch root radius  $r_0$  corresponding to  $\tau$  values are also indicated. For decreasing  $r_0$  (increasing notch severity), the time to failure is logically decreasing. This trend is observed for  $r_0 \geq 0.8\text{mm}$ , but the peculiar effect is the higher creep lifetime for  $r_0 = 0.45\text{mm}$ . [4]

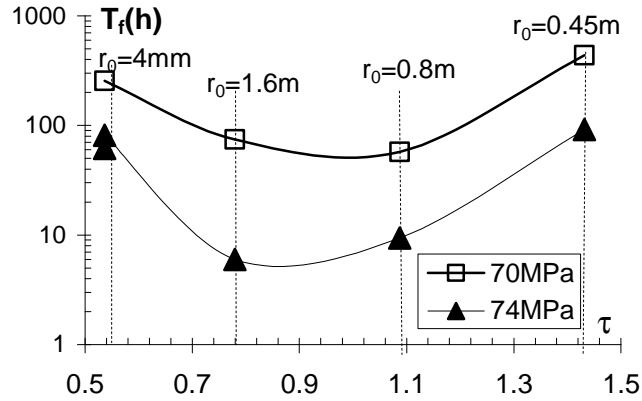


Figure 2: Time to failure versus stress triaxiality: higher creep lifetime for  $r_0 = 0.45\text{mm}$

To go further, a reference strain  $\varepsilon$  is introduced, based on the notch opening displacement  $\delta(t)$  measured during the test:

$$\varepsilon(t) = \frac{\delta(t) - \delta_L}{\delta_L} \quad (2)$$

In equation 2,  $\delta_L$  is the value of the notch opening displacement at the end of the loading stage. The strain rate  $d\varepsilon/dt$  is obtained by the time derivative of  $\varepsilon$ .

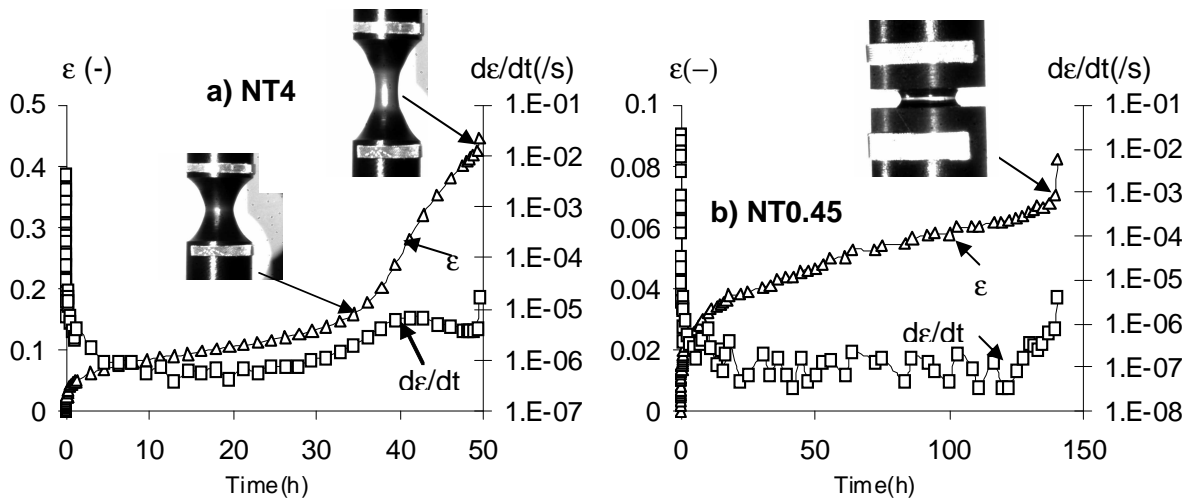


Figure 3: Creep strain and creep strain rate vs. creep time at 74MPa net stress: a) NT4; b) NT0.45

Figure 3 shows, for NT4 and NT0.45 specimens, the evolution with time of the creep reference strain and the creep strain rate. Additionally, some pictures indicating the general shape of the specimens were superimposed. Both figures correspond to net stress of about

74MPa and the two selected values of  $r_0$ , namely, 4mm and 0.45mm lead to extreme values of initial stress triaxiality whereas the creep lifetimes are roughly the same (see figure 2).

Figure 3a displays the creep strain and the creep strain rate history for NT4. The curve is divided into five stages that can be distinguished by the trends of the creep strain rate. The curve begins with classical primary and secondary-like creep stages where the creep strain rate is decreasing and stabilizes respectively. When the creep strain rate starts to increase again, it was noticed that necking together with a slight whitening appeared in the net section of the specimen. Next step corresponds to the extension of the necking zone, with an homogeneous whitening within this zone. Then, the creep strain decreases again, reo-hardening is assumed to occur here, before the final break of the specimen. This creep strain history is typical to notched specimens for which  $r_0 \geq 0.8\text{mm}$ .

Figure 3b is specific to NT0.45. Here, only three stages are depicted. The creep strain rate decreases, stabilizes and increases again before failure of the specimen. No necking is evidenced and the picture clearly shows that intense localized whitening appears in the net section. Furthermore, the magnitude of the creep strain for NT0.45 is very low compared with that of NT4.

**Fracture surfaces**

Regrain [5] performed interrupted creep tests on similar specimens of the same material. Specimens issued from those tests were longitudinally cryo-fractured and examined with a scanning electron microscope (SEM). It turned out that voids that were assumed to be pre-existing grow during the creep deformation. The location of the maximum void volume fraction depends on the initial value of  $\tau$ . One way to assess this distinction is to observe fracture surfaces of the broken specimens after the creep failure. The presence of dimples indicates initiation of the void growth process, assumed to be characteristic of a ductile fracture surface. Additional pictures of such a surface can be seen in figure 7. It was also noted that the brittle fracture surface was seemingly inter-spherulitic. Figure 4 summarizes the fracture surface patterns seen on each specimen. Additionally, the occurrence of observed necking was reported, depending on the initial notch root radius.

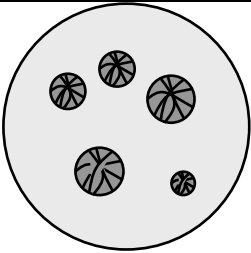
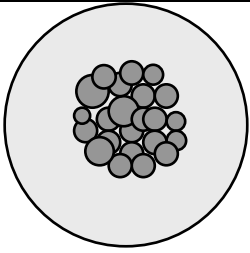
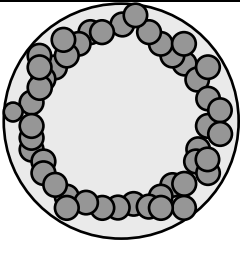
Sparse ductile surface	Diffuse ductile surface	Confined ductile surface	Brittle surface
			
Smooth $r_0 = 4 \text{ mm}$ $r_0 = 1,6\text{mm}$	$r_0 = 0,8\text{mm}$ $r_0 = 0,45\text{mm}$	$r_0 = 0,45\text{mm}$	
Necking	No necking		

Figure 4: Aspects of fracture surfaces and occurrence of necking according to the notch root radius.

NT4 and NT1.6 (left side of figure 4) showed sparse ductile surface. Very few dimples with elongated fibrils can be seen. It is presumably due to final failure under uniaxial conditions after highly stretched necking. For NT0.8 and few NT0.45, ductile surface pattern located in the centre of the net section is observed. Last, for most NT0.45 specimens, ductile fracture surface is confined next to the notch root. Accordingly, damage mechanisms are different between NT0.8 and NT0.45. This latter shows the classical configuration of an initially sharp crack even after blunting. In other words, the NT0.45 round bar can be assumed to be a pre-cracked specimen from fracture mechanics viewpoint.

To go further, fracture surfaces were analyzed by establishing the fraction of average ductile radius  $L_D$  with respect to the total radius of the net section ( $L_{tot}$ ). This is assumed to be the characteristic length of damaged material before failure. Thus, the definition for NT0.45 is specific in the sense that  $L_D$  includes the notch depth  $a$  (see figure 1).

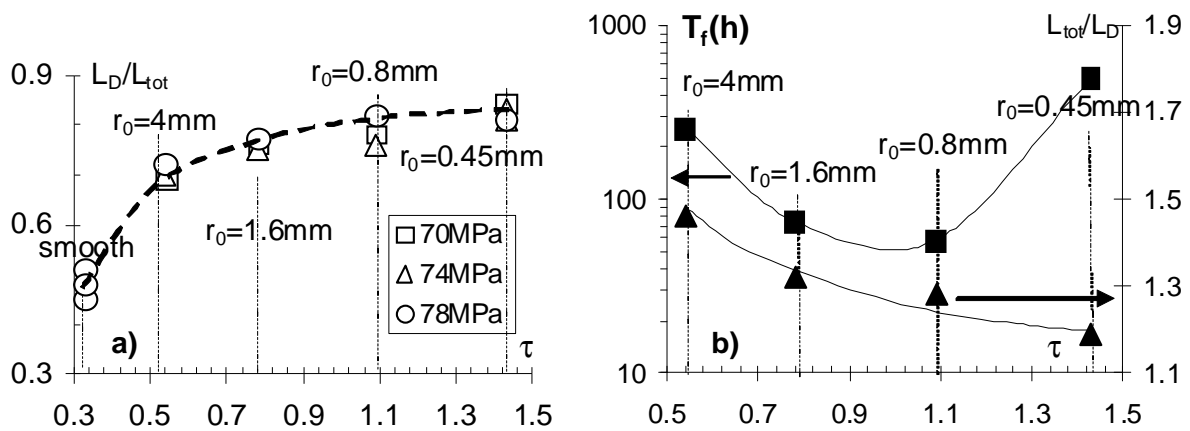


Figure 5: Ductile length fraction vs. stress triaxiality ratio  $\tau$ . a) for three applied net stresses; b) for 70MPa where the time to failure was superimposed.

By using these definitions, the ductile length fractions  $L_D/L_{tot}$  were plotted in figure 5a against  $\tau$ . Whatever the applied net stress, a continuous increase in this ductile fraction is observed for increasing  $\tau$ . Indeed, the higher the stress triaxiality, the higher the void growth rate, the larger the ductile surface. This latter remained printed on the fracture surface after the final brittle fracture.

In figure 5b, creep lifetime  $T_f$  was superimposed to the inverse of the ductile length fraction ( $L_{tot}/L_D$ ). The same trend is observed while  $r_0 \geq 0.8\text{mm}$ , i.e. when damage evolution starts from the centre towards the notch root. A peculiar deviation occurs when  $r_0 = 0.45\text{mm}$ , when the damage evolves from the notch root to the centre of the net section. As mentioned previously, this specimen is similar to a pre-cracked one, dedicated to fracture mechanics experimentations. The global approach of fracture mechanics is presumably applicable to experimental data on NT0.45.

## DISCUSSION

### Global approach

For creep tests on pre-cracked specimens, the fracture mechanics for creeping solids [6] suggests the use of  $C^*$  parameter so as to establish a master curve [2, 7].  $C^*$  is valid once

the specimen has reached the secondary creep stage. For circumferentially cracked round bars such as NT0.45, the  $C^*$  formula reads [2, 7]:

$$C^* = \left( \frac{n_2 - 1}{n_2 + 1} \right) \sigma_{\text{net}} \dot{\delta} \quad (3)$$

where  $n_2$  is the creep stress exponent,  $\sigma_{\text{net}}$  the applied net stress,  $\dot{\delta}$  is the minimum crack opening displacement rate, measured during the creep test.

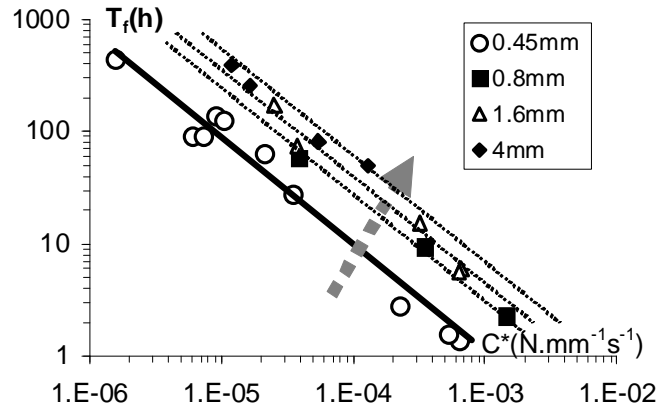


Figure 6: Time to failure vs.  $C^*$  master curve for PA6 at room temperature.

Figure 6 plots, with open circle symbols, time to failure ( $T_f$ ) against the value of  $C^*$  for NT0.45 specimens. The solid line represents the correlation line for pre-cracked specimens. A rather good agreement is observed for this correlation line. This latter, so-called master curve is useful for engineering determination of the creep lifetime of a structure made of PA6. Indeed, for a given cracked body (engineering component for instance), once the value of  $C^*$  is determined, the time to failure can be predicted via the master curve in figure 6.

In equation (3), it can be noticed that only  $b$  (net section radius) is taken into account via  $\sigma_{\text{net}}$ . The notch root radius does not interfere in  $C^*$  formula. Hence, by plotting data for all  $NTr_0$  specimens, the trend can be observed in figure 6. The grey dashed arrow indicates the way where the correlation lines move for increasing notch root radius. The higher the value of the notch root radius, the more significant the shift to the right of the correlation line. In fact, the effect of notch root radius is essentially attributed to the measured notch opening displacement rate  $\dot{\delta}$ . Accordingly,  $C^*$  continuously increases with  $r_0$ .

As observed in figure 6, the basic correlation (solid line) for NT0.45 logically predicts conservative lifetime for the other notch root radii specimens. It can then be used to keep a safety margin on the residual lifetime prediction. However, a master curve depending on the notch root radius can be criticized as being not intrinsic to the material. Furthermore, with the global approach of fracture mechanics, damage mechanisms, such as the location of the maximum porosity cannot be captured. This is the main motivation of the local approach of fracture described in the next section.

### Local approach to fracture: accounting for damage mechanisms

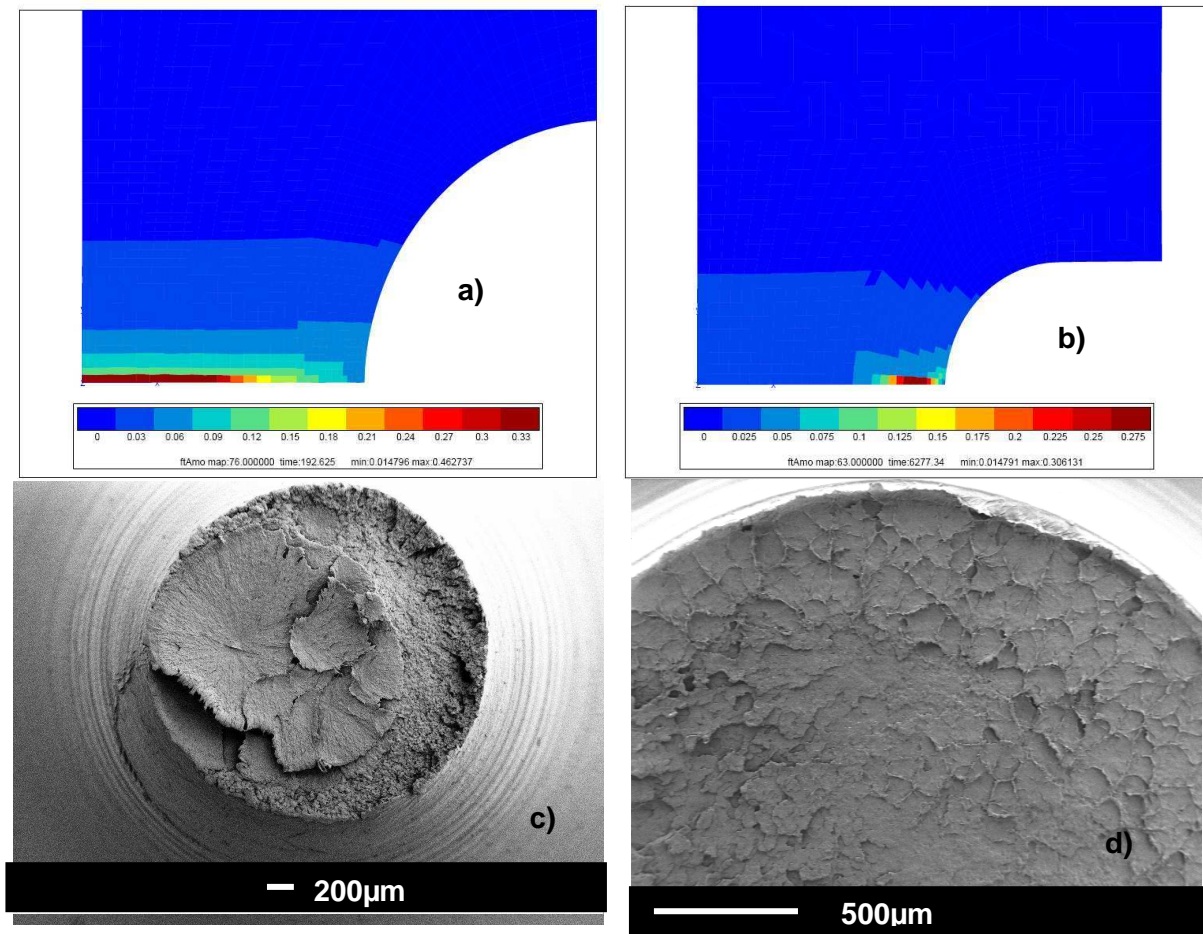


Figure 7: Comparison between damage contour map and fracture surfaces: a) and c) NT0.8, maximum porosity as well as ductile surface located in the centre; b) and d) NT0.45, maximum porosity and ductile surface next to the notch root.

To begin with, local approach of fracture is always associated to finite element analysis (FEA). Indeed, in order to assess local damage parameters on complex geometry under triaxial stress states, FEA is the common method to be used. The challenge here is the ability to capture damage mechanisms observed previously. To this end, the volume fraction of voids is assumed to be the damage parameter. The aim of the modelling is to assess both the amount of damage and the location of its maximum according to the applied net stress. FEA [8] requires robust constitutive equations able to account for various stress levels and triaxiality under creep load. The basis of a multi-mechanisms model –called 2M2C– is published elsewhere [1] and will not be presented here. The modified Gurson-Tvergaard-Needleman model [9-10] was coupled with the 2M2C model to account for the evolution of porosity. First results are presented in figure 7, where contour maps of damage are shown. Figure 7a and c shows that the maximum damage is located at the centre of the specimen for NT0.8 whereas figure 7b and d dedicated to NT0.45 capture the location of maximum damage near the notch root. Ductile fracture surfaces can be assessed via the void volume fraction parameter thanks to this local approach of fracture. Parameters such as the critical porosity have to be well optimized in order to simulate ductile tearing.

## CONCLUSION

An attempt was made to characterise the effect of stress triaxiality on the creep behaviour, damage and failure of PA6 at room temperature. To this end creep tests on notched round bars were carried out. Apart from an experimental database obtained for PA6 tested under creep at multiaxial stress state, microscopic examinations revealed the deformation, damage and failure mechanisms. Especially, depending on the notch root radius one can observe, either ductile failure started around the centre of the minimum cross section to continue with brittle failure at the surface (notch root), or crack initiation at free surface (near the notch root) and propagation towards the centre. The global approach of fracture mechanics for creeping solids cannot account for the aforementioned failure mechanisms. Alternatively, the local approach of fracture mechanics assisted by finite element analysis could successfully capture the key points of these creep failure mechanisms.

## REFERENCES

- [1] Regrain, C.; Laiarinandrasana, L.; Toillon, S. ; Sai, K.:  
Multi-mechanism models for semi-crystalline polymer: Constitutive relations and finite element implementation.  
International Journal of Plasticity 25(7) (2009), pp. 1253-1279.
- [2] Regrain, C.; Laiarinandrasana, L.; Toillon, S.:  
Experimental and numerical study of creep and creep rupture of PA6.  
Engineering Fracture Mechanics 76(18) (2009), pp. 2656-2665.
- [3] Bridgman, P. W.: 1944.  
The stress distribution at the neck of a tension specimen.  
Transactions ASM. 32 (1944), 553-574.
- [4] Regrain, C., Laiarinandrasana, L., Toillon, S.:  
Experimental and numerical study of behaviour, damage and crack propagation of PA6.  
Proceedings of 17<sup>th</sup> European Conference on Fracture , 2008, September 2-5, Brno, Czech Republic.
- [5] Regrain, C.:  
Experimental and numerical study of creep behaviour, damage and crack propagation of polyamide 6.  
PhD Thesis (*in French*), Ecole Nationale Supérieure des Mines de Paris 2009.
- [6] Riedel, H.; Rice, J.R.:  
Tensile cracks in creeping solids.  
Fracture Mechanics (1980) ASTM STP 700, pp. 112-130.
- [7] Ben Hadj Hamouda, H.; Laiarinandrasana, L.; Piques, R.:  
Fracture mechanics global approach concepts applied to creep slow crack growth in a Medium Density PolyEthylene (MDPE)  
Engineering Fracture Mechanics 74(14) (2007), pp. 2187-2204.
- [8] Besson, J.; Foerch, R.:  
Large scale object-oriented finite element code design  
Computer Methods in Applied Mechanics and Engineering 142 (1997), pp. 165-187
- [9] Gurson, A.L.:  
Continuum theory of ductile rupture by void nucleation and growth: Part 1 yield criteria and flow rules for porous ductile media.  
J. Eng. Mater Technol. 99 (1977), pp. 2-15.
- [10] Tvergaard, V., Needleman, A.:  
Analysis of the cup-cone fracture in a round tensile bar.  
Acta Metall. 32 (1984), pp. 157-169.

**Corresponding author:** lucien.laiarinandrasana@mines-paristech.fr